The Nonlinear Dynamics of Time-Dependent Subcritical Baroclinic Currents

G. R. FLIERL

Department of Earth, Atmospheric, and Planetary Sciences, Massachusetts Institute of Technology, Cambridge, Massachusetts

J. PEDLOSKY

Department of Physical Oceanography, Woods Hole Oceanographic Institution, Woods Hole, Massachusetts

ABSTRACT

The nonlinear dynamics of baroclinically unstable waves in a time-dependent zonal shear flow is considered in the framework of the two-layer Phillips model on the beta plane. In most cases considered in this study the amplitude of the shear is well below the critical value of the steady shear version of the model. Nevertheless, the time-dependent problem in which the shear oscillates periodically is unstable, and the unstable waves grow to substantial amplitudes, in some cases with strongly nonlinear and turbulent characteristics. For very small values of the shear amplitude in the presence of dissipation an analytical, asymptotic theory predicts a self-sustained wave whose amplitude undergoes a nonlinear oscillation whose period is amplitude dependent. There is a sensitive amplitude dependence of the wave on the frequency of the oscillating shear when the shear amplitude is small. This behavior is also found in a truncated model of the dynamics, and that model is used to examine larger shear amplitudes. When there is a mean value of the shear in addition to the oscillating component, but such that the total shear is still subcritical, the resulting nonlinear states exhibit a rectified horizontal buoyancy flux with a nonzero time average as a result of the instability of the oscillating shear. For higher, still subcritical, values of the shear, a symmetry breaking is detected in which a second cross-stream mode is generated through an instability of the unstable wave although this second mode would by itself be stable on the basic time-dependent current. For shear values that are substantially subcritical but of order of the critical shear, calculations with a full quasigeostrophic numerical model reveal a turbulent flow generated by the instability. If the beta effect is disregarded, the inviscid, linear problem is formally stable. However, calculations show that a small degree of nonlinearity is enough to destabilize the flow, leading to large amplitude vacillations and turbulence. When the most unstable wave is not the longest wave in the system, a cascade up scale to longer waves is observed. Indeed, this classically subcritical flow shows most of the qualitative character of a strongly supercritical flow. This result supports previous suggestions of the important role of background time dependence in maintaining the atmospheric and oceanic synoptic eddy field.

1. Introduction

Although the classical theory of the instability of zonal flows on the beta plane gives clear thresholds required for instability, time-dependent flows can exhibit instability when their shears are below the classical critical values. Recent work by Poulin et al. (2003) for the problem of barotropic instability and Pedlosky

and Thomson (2003, hereinafter PT03) for near-critical baroclinic instability each demonstrate the possibility for vigorous parametric instability for flows whose steady counterparts are stable. Parametric instability arises when the frequency of the basic flow matches a multiple characteristic frequency of an otherwise stable perturbation.

The work of Farrell and Ioannou (1999) shows the deep connection in the linear version of the problem between the parametric instability and the general theory of nonnormal generation of perturbations and points out (as did PT03) how the presence of time dependence of the basic state weakens the necessary con-

ditions for instability, allowing instability for shears that would be otherwise stable. The attention of our study here, however, is to focus on the nonlinear behavior of the perturbations that arise from the parametric instability. We study the dynamics of baroclinic instabilities in the Phillips (1954) two-layer model on the beta plane and consider parameter values such that the basic state would be well below the threshold for instability in that model were it steady. We demonstrate a wide range of finite-amplitude and turbulent behavior, all present in flows which by any classical criterion would be considered stable. This has obvious implications for parameterizations of eddy development in large-scale circulation models that use a criticality condition to determine a threshold for the presence and strength of eddy activity.

In section 2 we present our quasigeostrophic model. In the third section we discuss an analytical theory for finite-amplitude perturbations on weak but oscillating shears that clearly illustrates the possibility for instability for shears well below the classical critical value. In section 4 we introduce a truncated modal version of the two-layer problem that we use to go beyond the formal asymptotics of section 3 to describe the role of mean shear on the fluxes generated by the disturbances. Section 5 describes a truncation allowing several modes with which we demonstrate the symmetry breaking for larger, but still subcritical, shears in which a meridional asymmetry develops in the perturbation and the correction to the mean zonal flow. The results of these sections are compared with calculations done with a full numerical version of the quasigeostrophic model in section 6. Strongly turbulent end states can appear, again for classically stable values of the shear. Section 6 also describes the nonlinear cascade to longer wavelengths when the most destabilized wave is not the largest wave possible in the periodic channel.

In section 7 we describe the behavior of the instability for $\beta = 0$. The linear inviscid problem for a purely oscillating shear is formally always stable in this case, but we demonstrate that the addition of nonlinearity destabilizes the flow although it still provides a finite-amplitude limit to the growth of the disturbance. We summarize and present our conclusions in section 8.

2. The model

We consider the Phillips (1954) two-layer model on the beta plane in which a zonal flow with vertical, but no horizontal, shear is confined in a channel of width L. The layer thicknesses in the absence of motion are assumed each to be equal to D for the sake of simplicity. If ψ_n is the geostrophic streamfunction in each layer, where $n = 1$ refers to the upper layer and $n = 2$ to the lower layer, the nondimensional governing equations are (Pedlosky 1987)

$$\frac{\partial}{\partial t} q_n + J(\psi_n, q_n) + \beta \frac{\partial \psi_n}{\partial x} = -\mu q_n, \quad n = 1, 2,$$

(2.1a)

where

$$q_n = \nabla^2 \psi_n + (-1)^n F(\psi_1 - \psi_2), \quad F = \frac{f_o^2 L^2}{g' D}, \quad \text{and}$$

$$\beta = \frac{\beta_{\mathrm{dim}} L^2}{U_{\mathrm{scale}}}.$$

(2.1b–d)

The nondimensional parameters F and β are defined respectively in terms of the ratio of channel width to deformation radius and planetary vorticity gradient to a characteristic value of the relative vorticity gradient and both are assumed to be $O(1)$. The operator J is the Jacobian of the two sequential functions with respect to x and y.

We consider perturbations to a shear $U_s = U_1 - U_2$ and, with no loss of generality, take $U_1 = -U_2 = U_s/2$ so that there is no mean barotropic flow in the basic state. We have also introduced a simple dissipation mechanism on the right-hand side of (2.1a) as a damping of potential vorticity with a rate constant μ.

Perturbations to the basic flow are described by $\phi_n(x, y, t)$ such that the total streamfunction is

$$\psi_n = (-1)^n y U_s/2 + \phi_n,$$

(2.2)

while the governing equations for the perturbations are

$$\left[\frac{\partial}{\partial t} - (-1)^n \frac{U_s}{2} \frac{\partial}{\partial x} + \mu\right] [\nabla^2 \phi_n + (-1)^n F(\phi_1 - \phi_2)] + \frac{\partial \phi_n}{\partial x} [\beta - (-1)^n F U_s] + J[\phi_n, \nabla^2 \phi_n + (-1)^n F(\phi_1 - \phi_2)] = 0.$$

(2.3)

If U_s were independent of time, the critical value required for growth of perturbations in the absence of dissipation would be β/F (Pedlosky 1987). With the potential vorticity damping in (2.3) the critical value is somewhat higher by $O(\mu)$. However, our interest is in situations where the basic shear is time-dependent and always less than this critical value. We will examine basic states of the form

$$U_s = \frac{\beta}{F}(G + H \cos\omega t),$$

(2.4)

such that $G + H < 1$: the shear at every instant is below the critical threshold.

It is helpful to reformulate the problem in terms of the barotropic and baroclinic modes of the perturbation fields. With the definitions

$$\phi_t = \frac{\phi_1 + \phi_2}{2} \quad \text{and} \quad \phi_c = \frac{\phi_1 - \phi_2}{2} \quad \text{(2.5a, b)}$$

for the barotropic and baroclinic modes, respectively, we obtain from (2.3)

$$\left(\frac{\partial}{\partial t} + \mu\right)(\nabla^2\phi_c - 2F\phi_c) + \frac{U_s}{2}\frac{\partial}{\partial x}(\nabla^2\phi_t + 2F\phi_t) + \beta\frac{\partial\phi_c}{\partial x} + J(\phi_t, q_c) + J(\phi_c, q_t) = 0, \qquad (2.6a)$$

$$\left(\frac{\partial}{\partial t} + \mu\right)\nabla^2\phi_t + \frac{U_s}{2}\frac{\partial}{\partial x}\nabla^2\phi_c + \beta\frac{\partial\phi_t}{\partial x} + J(\phi_t, q_t) + J(\phi_c, q_c) = 0, \quad q_t \equiv \nabla^2\phi_t, \quad \text{and} \quad q_c = \nabla^2\phi_c - 2F\phi_c.$$

$$(2.6b\text{–}d)$$

We define the perturbation energy density E:

$$E = \frac{1}{2}\left[(\nabla\phi_1)^2 + (\nabla\phi_2)^2 + F/2(\phi_1 - \phi_2)^2\right]$$

$$= (\nabla\phi_t)^2 + (\nabla\phi_c)^2 + 2F\phi_c^2, \qquad (2.7)$$

leading to the perturbation energy equation:

$$\left(\frac{\partial}{\partial t} + 2\mu\right)\langle E\rangle = 2FU_s\left\langle\phi_c\frac{\partial\phi_t}{\partial x}\right\rangle, \qquad (2.8)$$

where the angle brackets refer to an integral over the channel width and over a wavelength of the perturbation. It is important to note that the energy release to the perturbations is given by the thickness flux of the perturbations in the presence of the shear, exactly as if the shear were steady.

We will from time to time use the enstrophy as a measure of the perturbation amplitude. It can similarly be defined in terms of the barotropic and baroclinic modes as

$$V = \frac{1}{2}\langle q_1^2 + q_2^2\rangle = \langle q_c^2 + q_t^2\rangle. \qquad (2.9)$$

The full numerical model solves the fluctuating potential vorticity equations

$$\frac{\partial}{\partial t}q_n' + \frac{\partial}{\partial x}(U_n q_n' + u_n' q_n') + \frac{\partial}{\partial y}(v_n' q_n' - \overline{v_n' q_n'})$$
$$+ Q_{ny}v_n' q_n' = -\mu q_n', \quad \text{with} \qquad (2.10)$$

$$q_n' = \nabla^2\psi_n' + (-1)^n F(\psi_1' - \psi_2'), \quad (2.11)$$

where an overbar denotes a zonal average. We use a pseudospectral method, with q_n' and ψ_n' expanded in exp $(imk_0 x)\sin(n\pi y)$ series. The zonal average flows evolve according to

$$\frac{\partial}{\partial t}U_n = \overline{v_n' q_n'} + \mathfrak{I}_n - \mu U_n + (-1)^{n+1}F\phi, \qquad (2.12)$$

where $\mathfrak{I}_n$ is the direct momentum forcing, for example, an applied stress for the upper layer, and ϕ is related to the transformed Eulerian mean (TEM) meridional circulation by

$$f_0\overline{v_n^*} = (-1)^n F\phi.$$

See, for example, Shepherd (1983) for a full discussion of the TEM formalism for the two-layer model.

An omega equation,

$$\left(\frac{\partial^2}{\partial y^2} - 2F\right)\phi = \frac{g'\partial\Theta}{f_0\partial y} + \mathfrak{I}_1 - \mathfrak{I}_2 + \overline{v_1' q_1'} - \overline{v_2' q_2'}$$

$$(2.13)$$

(with Θ being the heating that causes transport across the interface) predicts the transformed mean circulation.

The background oscillating state,

$$\overline{U_n} = (-1)^{n+1(1/2)}[G + H\sin(\omega t)],$$

can be produced by suitable choices of $\mathfrak{I}_1$, $\mathfrak{I}_2$, and Θ; the remaining part of the mean flows and meridional circulations (which are forced by the eddy PV fluxes and the damping) satisfy $U_n' = \phi = 0$ on the walls. Therefore, we can use $\sin(n\pi y)$ series for those, making the inversion of the omega equation as straightforward as that used for the q_n' equation. The background PV gradient is computed from the zonal mean

$$Q_{ny} = \beta - U_{nyy} + (-1)^{n+1}F(U_1 - U_2)$$

and includes both the specified latitude-independent part and the sine series part.

Most of the calculations are done with a 2-to-1 aspect ratio for the channel and 128 (65) points in x (y). Time stepping begins with two second-order Runge–Kutta steps and then continues with a third-order Adams–Bashforth scheme.

3. The small H limit

It proves illuminating to examine first the dynamics of the instability when the amplitude of the oscillating shear is very small. We shall start in the case when $G = 0$, that is, no mean shear, and for values of $H \ll 1$ so that the flow, at each instant, is far less than the critical value β/F. Without loss of generality we will take this critical value to be 1 and note that this just defines the scaling velocity for the shear to be $\beta_{\dim}(g'D)/f_o^2$, that is, the Rossby long-wave speed. When there is no shear, the solutions to (2.6a, b) will be the two Rossby wave modes of undetermined amplitude, and we anticipate that for small shear, if unstable, the waves will slowly grow on a time scale that depends on the shear, or H.

We assume an amplitude expansion for each stream-function,

$$\phi_{c,t} = a[\phi_{c,t}^{(0)} + a\phi_{c,t}^{(1)} + \cdots], \tag{3.1}$$

and introduce the slow, development time

$$T = Ht, \tag{3.2}$$

assuming that $a = O(H^{1/2})$ and $\mu = O(H)$, and defining $\tilde{\mu} = \mu/H$. We allow the geostrophic streamfunctions to be functions of both t and T so that the time derivatives in (2.6) are transformed as

$$\frac{\partial}{\partial t} \Rightarrow \frac{\partial}{\partial t} + H\frac{\partial}{\partial T}.$$

The expansion in amplitude and the ordering relations as described yield the following sequence of problems.

At lowest order we obtain the equation of the barotropic and baroclinic Rossby modes. It proves convenient to express the solutions as

$$\phi_t^{(o)} = B_t(t, T)e^{ikx}e^{-ikt(c_c+c_t)/2}\sin ly + * \quad \text{and} \tag{3.3a}$$

$$\phi_c^{(o)} = B_c(t, T)e^{ikx}e^{-ikt(c_c+c_t)/2}\sin ly + *, \tag{3.3b}$$

where an asterisk denotes complex conjugation, and

$$c_t = -\frac{\beta}{K^2}, \quad c_c = -\frac{\beta}{K^2 + 2F},$$

$$K^2 = k^2 + l^2, \quad \text{and} \quad l = m\pi. \tag{3.4a–d}$$

The y wavenumber has been chosen as an integral multiple of π to satisfy the condition of no normal flow at the channel boundary. In the following we will choose the lowest, most unstable mode, $m = 1$. The governing equations for the amplitude variables $B_{c,t}$ have the useful symmetry

$$\left.\begin{array}{l} \dfrac{\partial}{\partial t}B_c - ik\dfrac{c_t - c_c}{2}B_c = 0, \\[2ex] \dfrac{\partial}{\partial t}B_t + ik\dfrac{c_t - c_c}{2}B_t = 0 \end{array}\right\} \Rightarrow B_t = B_{to}(T)e^{-i\sigma t}, B_c = B_{co}(T)e^{i\sigma t}$$

$$\sigma = k\frac{c_t - c_c}{2}. \tag{3.5}$$

The frequency σ is the critical frequency for defining resonance with the oscillating shear for parametric instability. At this order, the two waves propagate as free Rossby waves; as we shall see, parametric instability occurs when the beat frequency, 2σ, matches the forcing frequency. Note that the wave amplitudes are still arbitrary functions of the long time variable, T, at this point.

At the next order in a the nonlinear terms provide a forcing only in the baroclinic equation in (2.6a) and the forcing is independent of x; that is,

$$\phi_t^{(1)} = 0 \quad \text{and}$$
$$\phi_c^{(1)} = \Phi(y, t, T), \tag{3.6}$$

and Φ satisfies

$$\frac{\partial}{\partial t}(\nabla^2\Phi - 2F\Phi) = 2iklF\sin 2ly(B_t B_c^* - B_t^* B_c). \tag{3.7}$$

The solution for Φ can be written, using the results of (3.5),

$$\Phi = P(t)\left(\frac{-2Fl}{4l^2 + 2F}\right)\left\{\sin 2ly - \frac{2l}{(2F)^{1/2}}\frac{\sinh[(2F)^{1/2}(y - 1/2)]}{\cosh(F/2)^{1/2}}\right\} \quad \text{and} \quad P = \frac{-k}{2\sigma}(B_{to}B_{co}^* e^{-2i\sigma t} + B_{to}^* B_{co}e^{2i\sigma t}), \tag{3.8a, b}$$

where we have used the boundary condition $\partial \Phi / \partial y = 0$, $y = 0, 1$ (Pedlosky 1987). Note that this correction to the mean flow oscillates with 2 times the frequency σ and contains no time means over a period of the oscillation. In the absence of a time mean value of the basic shear there is no direction in y chosen by the shear and, hence, we do not expect that the thickness fluxes in the unstable waves, leading to a correction to the baroclinic flow, can choose a direction for a rectified flux that can produce a time-averaged mean flow correction. In the next section we will examine the mean flow corrections produced when there is a mean, but subcritical, basic-state shear.

When proceeding to the next order in the a expansion, we obtain a linear problem for the higher order corrections to the geostrophic streamfunction. When the projection on modes with the x and y form $e^{ikx} \sin ly$ of the lowest-order eigenfunction are considered, the resulting time-dependent problem has the form of (3.5) in which some of the terms on the right-hand sides oscillate with the natural frequencies of the linear operators of the left-hand side. Eliminating such terms, which would contribute secularly growing terms in our expansion and so render it otherwise invalid, yields the following equations in the long time variable T for the amplitudes of the lowest-order Rossby waves:

$$\left(\frac{\partial}{\partial T} + \tilde{\mu} \right) B_{to} + \frac{\beta}{2F} \frac{ik}{2} B_{co} - \frac{ik}{2\sigma} N_1 B_{to} |B_{co}|^2 = 0,$$

(3.9a)

$$\left(\frac{\partial}{\partial T} + \tilde{\mu} \right) B_{co} - \frac{\beta}{2F} \frac{ik}{2} R B_{to} + \frac{ik}{2\sigma} N_2 B_{co} |B_{to}|^2 = 0,$$

(3.9b)

and

$$R = \frac{2F - K^2}{2F + K^2}.$$

(3.9c)

In suppressing terms that are possibly resonant against the linear operators in (3.5) it is necessary that the basic shear oscillate at a frequency: $\omega = 2\sigma = k(c_t - c_c)$. If not, the second term in both (3.9a) and (3.9b) that comes from the interaction of the oscillating shear and the lowest-order Rossby waves would not appear. The constants N_1 and N_2 result from the projection of the nonlinear interaction terms between the basic wave and the correction to the mean flow and are given in appendix A. The nonlinear system (3.9a, b) governs the amplitude of the Rossby waves of (3.3a, b) and thus also describes, using (3.8), the correction to the mean zonal flow.

If the nonlinear terms in (3.9) are momentarily ne-glected we can use the remaining linear terms to discuss the stability of the Rossby waves and, hence, their ability to grow on the oscillating shear. This yields the behavior expected when the small-amplitude perturbations begin to grow (if they are unstable). Looking for solutions of the form $e^{\alpha T}$, or equivalently $e^{\alpha Ht}$, yields a growth rate:

$$\alpha H = \frac{k\beta}{4F} HR^{1/2} - \mu.$$

(3.10)

Thus the oscillating shear is unstable for amplitudes that exceed

$$H_{\text{crit}} = \frac{\mu 4F}{\beta k} \left(\frac{2F + K^2}{2F - K^2} \right)^{1/2},$$

(3.11)

which shares the same short-wave cutoff as the standard steady problem. The requirement that the frequency of the shear flow be exactly 2σ can be relaxed, as discussed below, and, in general, for larger H the range of frequencies for which this parametric instability arises is expanded.

After a time interval of exponential growth the nonlinear terms in (3.9a, b) can no longer be ignored. Nonlinear solutions of (3.9a, b) can nonetheless be found. They are not steady solutions but periodically oscillate with the long time variable T. Thus with

$$B_{to} = B'_{to} e^{i\varpi T} \quad \text{and} \quad B_{co} = B'_{co} e^{i\varpi T}$$

(3.12a, b)

examination of the real and imaginary parts of (3.9a, b) after multiplication by the complex conjugates of the barotropic and baroclinic amplitudes leads to

$$|B_{to}|^2 = |B_{co}|^2 / R \quad \text{and}$$

(3.13a)

$$\varpi = \frac{k}{4\sigma} |B_{co}|^2 (N_1 - N_2 / R),$$

(3.13b)

which when inserted into (3.9a, b) yield the amplitude of the oscillation,

$$|B_{co}|^2 = \frac{4\sigma}{k} \left[\frac{\left(\frac{k^2 \beta^2 R}{16F^2} - \tilde{\mu}^2 \right)^{1/2}}{|N_1 + N_2 / R|} \right].$$

(3.14)

It is important to note that according to (3.10) and (3.14) a finite-amplitude solution is possible only when the linear solution is unstable. Also, the final state is predicted from (3.13b) to contain a frequency shift that is directly proportional to the square of the equilibrated amplitude. Figure 1 shows the development on the slow time T of the initial instability and its equilibration. Figure 1a shows the real and imaginary parts of the barotropic amplitude, Fig. 1b the baroclinic amplitude. After a period of exponential growth the solution
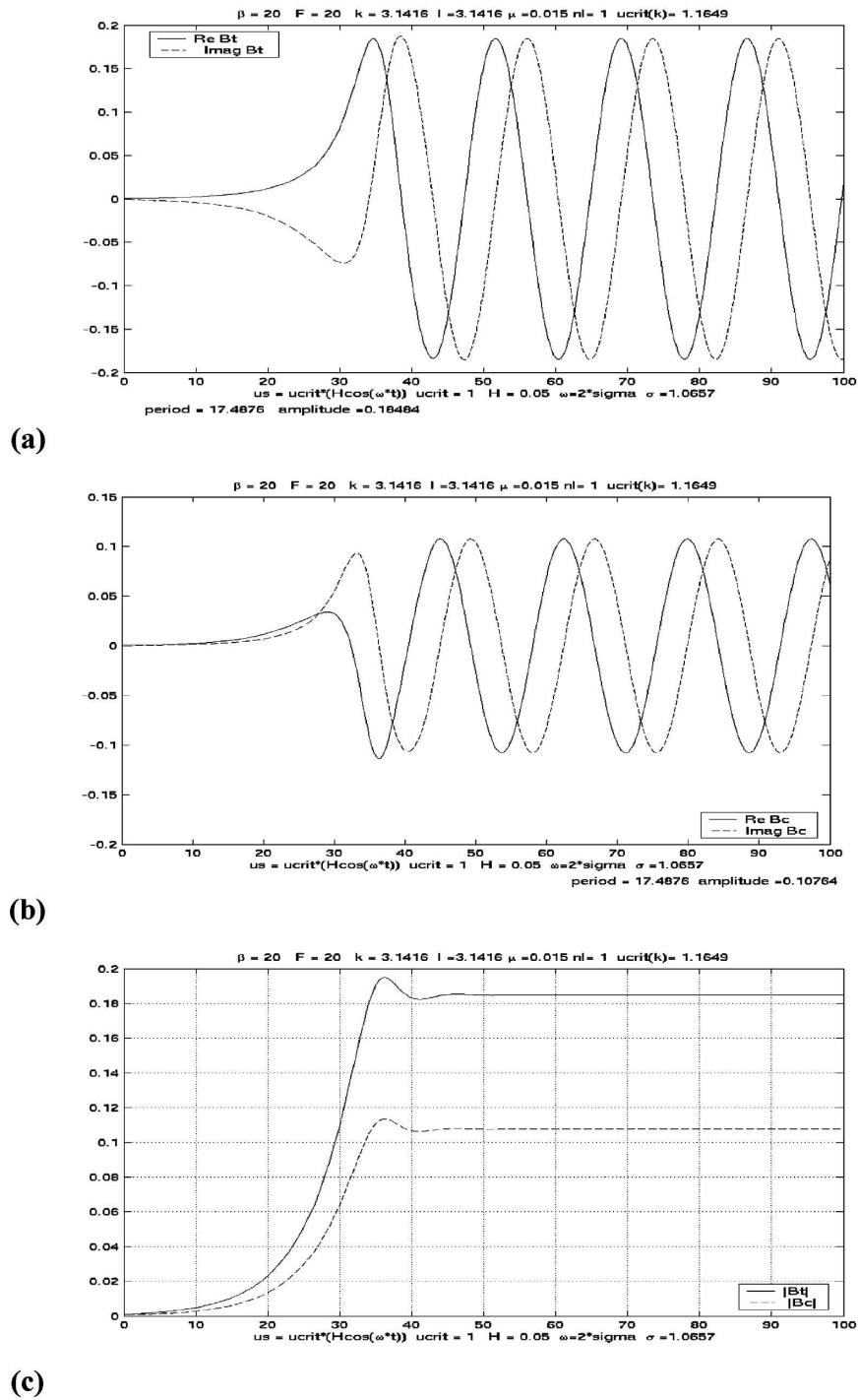
(a)

(b)

(c)

FIG. 1. The asymptotic, small H solutions developing on the long time scale $T = Ht$: (a) The real and imaginary parts of the barotropic Rossby wave amplitude and (b) for the baroclinic amplitudes. In each case the results match those of the analytic solutions of (3.13) and (3.14). (c) The evolution of the absolute value of the amplitudes. The calculations are done for $\mu = 0.015$, $F = \beta = 20$, $H = 0.05$, and $k = l = \pi$.
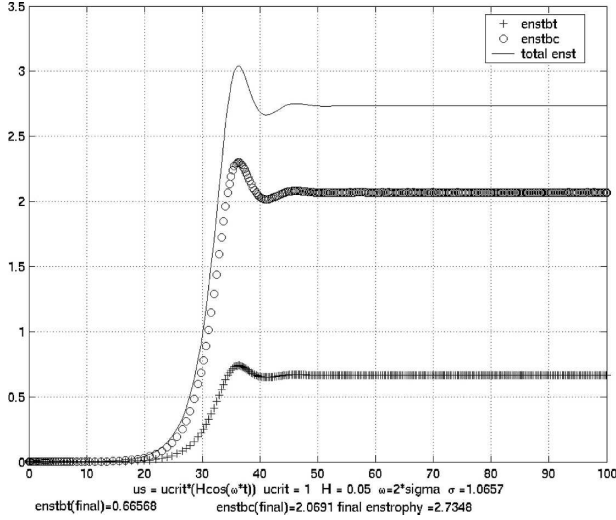
FIG. 2. The asymptotic small H solution for the enstrophy of the unstable waves showing the baroclinic, barotropic, and total enstrophy. Parameters are as in Fig. 1.
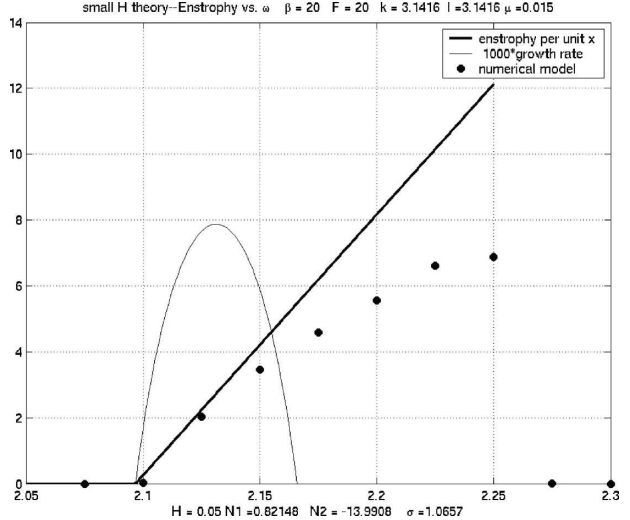

FIG. 3. The equilibrated enstrophy for $H \ll 1$ as a function of frequency. The straight line shows the enstrophy. The arc is the linear growth rate $\times$ 10^3. The dark circles show the results from the fully nonlinear quasigeostrophic numerical model.

settles into an oscillation, as predicted from (3.13) and (3.14). The wave amplitude equilibrates to a steady value, see Fig. 1c, while the frequencies shift by the nonlinear correction, ϖ, given by (3.13). Figure 2 shows the development and equilibration of the enstrophy of the wave field in which the period of exponential growth is clear, followed by an equilibration to a steady value for each component. It is not difficult to show that in the equilibrated state the energy equation (2.8) describes a finite-amplitude state in which the wave continues to extract energy from the oscillating basic shear, and that energy extraction is associated with an oscillating thickness flux that rectifies its product with the shear. The resulting energy extraction is then exactly balanced by dissipation.

It is not difficult to repeat the above analysis allowing a slight mismatch between the frequency of the oscillating shear and σ. Writing

$$\omega = 2\sigma + H\delta, \tag{3.15}$$

the equations for the lowest-order Rossby wave amplitudes become

$$\left(\frac{\partial}{\partial T} + \tilde{\mu}\right)B_{to} + \frac{\beta}{2F}\frac{ik}{2}B_{co}e^{-i\delta T} - \frac{ik}{2\sigma}N_1 B_{to}|B_{co}|^2 = 0, \tag{3.16a}$$

and

$$\left(\frac{\partial}{\partial T} + \tilde{\mu}\right)B_{co} - \frac{\beta}{2F}\frac{ik}{2}RB_{bo}e^{i\delta T} + \frac{ik}{2\sigma}N_2 B_{co}|B_{to}|^2 = 0. \tag{3.16b}$$

Again, solutions can be found in the form

$$B_{co} = B'_{co}e^{i\varpi T} \quad \text{and} \quad B_{to} = B'_{to}e^{i(\varpi - \delta)T}. \tag{3.17a, b}$$

The detuning of the shear flow frequency by an amount δ alters the linear instability, and repeating the linear analysis as before leads to a prediction of linear growth rate in the linear regime,

$$\text{Im}(\varpi) = \left(\frac{\beta^2 k^2 R}{16F^2} - \frac{\delta^2}{4}\right)^{1/2} - \tilde{\mu}, \tag{3.18}$$

so that sufficient detuning will stabilize the perturbation. On the other hand, an analysis similar to that leading to (3.14) now yields

$$|B_{co}|^2 = \frac{4\sigma}{k}\left[\frac{\left(\frac{k^2\beta^2 R}{16F^2} - \tilde{\mu}^2\right)^{1/2}}{|N_1 + N_2/R|} + \frac{\delta}{2|N_1 + N_2/R|}\right]. \tag{3.19}$$

As a function of frequency the condition for the existence of finite-amplitude solutions is not identical to the condition for instability. The low-frequency cutoff (δ negative) is the same, but for positive δ the prediction of the theory is for the amplitude to increase with increasing frequency. Figure 3 shows the equilibrated total enstrophy per unit x as a straight line, while the arc in the figure is the growth rate (multiplied by 10^3). The left-hand, low-frequency cutoff for instability corresponds to the cutoff of finite-amplitude solutions. They

exist only for frequencies that make the square bracket in (3.19) positive. On the other hand, the prediction of the theory is for the amplitude to continue to grow beyond the region of linear instability. The theory has been checked using a fully nonlinear quasigeostrophic model (described in section 5) and the results are shown by the full circles in the figure. For small differences of the frequency from σ there is good agreement and, as expected, when the frequency difference becomes larger the numerical results diverge quantitatively from the asymptotic theory. However, the qualitative nature of the result is identical. The implication is that nonlinearity is destabilizing in the frequency interval beyond that predicted by (3.18). This prediction is also reproduced by the truncated modal model described in the next section. It is important to note that the predicted amplitude is $O(H)^{1/2}$ so that for small H the amplitude can remain substantial until H becomes very small.

4. The truncated model (single wave)

To go beyond the parameter range for which the small H theory is valid, we have found it useful to consider a solution to (2.6) truncated to a single wave mode plus a mean flow correction,

$$\phi_c = A_c(t)e^{ikx}\sin ly + * + \Phi(y, t) \quad \text{and} \quad (4.1a)$$

$$\phi_t = A_t(t)e^{ikx}\sin ly + *. \quad (4.1b)$$

Taking the x average of (2.6a) leads to

$$\left(\frac{\partial}{\partial t} + \mu\right)\left(\frac{\partial^2 \Phi}{\partial y^2} - 2F\Phi\right) = 2iklF\sin 2ly\,(A_t A_c^*$$

$$- A_t^* A_c). \quad (4.2)$$

Again, we can find solutions for Φ in the form of (3.8), essentially similar to (3.8); that is,

$$\Phi = P(t)\left(\frac{-2Fl}{4l^2 + 2F}\right)$$

$$\times \left\{\sin 2ly - \frac{2l}{(2F)^{1/2}}\frac{\sinh[(2F)^{1/2}(y - 1/2)]}{\cosh(F/2)^{1/2}}\right\},$$

$$(4.3)$$

where $P(t)$ satisfies

$$\left(\frac{\partial}{\partial t} + \mu\right)P = ik(A_t A_c^* - A_t^* A_c), \quad (4.4)$$

while the amplitudes are determined by inserting (4.1a, b) into (2.6) and considering the projection of the resulting terms on the spatial wave functions $e^{ikx}\sin ly$ to obtain

$$\left(\frac{d}{dt} + \mu\right)A_t = -\frac{ikU_s}{2}A_c + ik\frac{\beta}{K^2}A_t - iA_cPN_1 \quad \text{and}$$

$$(4.5a)$$

$$\left(\frac{d}{dt} + \mu\right)A_c = \frac{ikU_s}{2}RA_t + ik\frac{\beta}{K^2 + 2F}A_c + iA_tPN_2,$$

$$(4.5b)$$

where R, N_1, and N_2 are defined by (3.9c) and (A.1a, b).

For small H and $G = 0$, the integration of (4.4) and (4.5) give results nearly identical to the predictions of small H theory of the preceding section. For example, Fig. 4a shows the evolution of the enstrophy for $H = 0.05$ from (4.4) and (4.5) for $\omega = 2\sigma$ and $G = 0$. The equilibrated value of the enstrophy (per unit x) is 2.789 according to the truncated model and this agrees well with the final value given by the small H theory (2.7345). Similarly, the prediction of the dependence on frequency of the enstrophy matches that of the asymptotic small H theory, as shown in Fig. 4b. The nearly linear increase in enstrophy begins at the critical frequency as determined by (3.18) and, as predicted, extends beyond the high-frequency cutoff of linear theory. Figure 4b is constructed as the result of many separate calculations and the final values of enstrophy are indicated either by an asterisk or a plus sign. The former are the result of calculations in which the initial conditions of the wave amplitudes are very small (10^{-3}). At some frequency near the high-frequency cutoff of linear theory those initial conditions do not produce a nontrivial finite-amplitude solution. However, if the calculation is initiated using as initial conditions the equilibrium solution corresponding to the finite-amplitude state at a slightly lower frequency, the new finite-amplitude solution is obtained. It follows that there are two solutions for such frequencies beyond the high-frequency cutoff; that is, either a zero-amplitude solution or a finite-amplitude solution that requires a finite-amplitude initial condition to reach it. In this range the parametric instability is, in fact, a finite-amplitude instability.

The asymptotic analytical solution for small H is developed in section 3 for $G = 0$. When G is not zero: that is, when there is a time mean shear, it is no longer possible to insist that the correction to the mean zonal flow have zero mean over a period of the oscillation; that is, there is not an added constant or function of slow time added to (3.8b). The single-mode truncation is a simple tool to examine this question. Its significance is connected to the thickness flux in the unstable wave. From the energy equation (2.8) this flux is proportional to
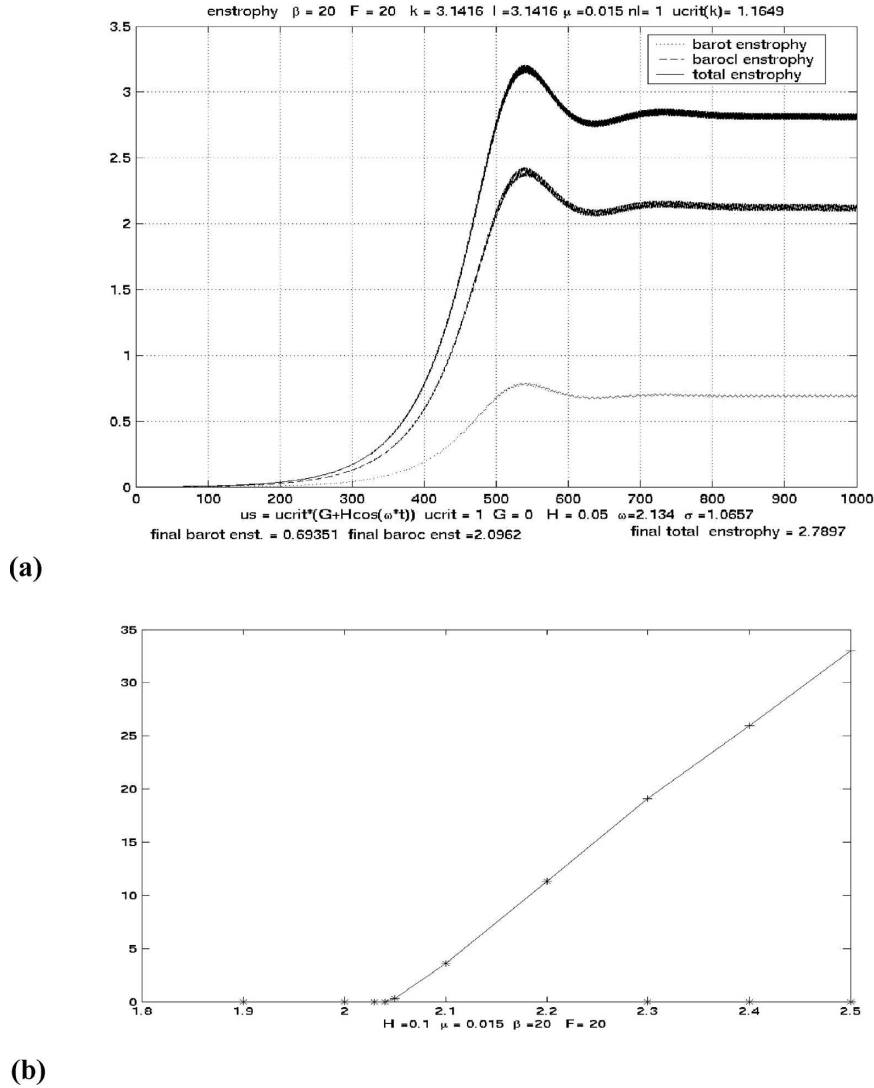
(a)

(b)

FIG. 4. (a) The evolution of the barotropic, baroclinic, and total enstrophy using the single-mode truncated model for the parameters of Fig. 1. (b) The enstrophy vs frequency from the truncated model.

$$\langle \phi_c \, \partial \phi_t / \partial x \rangle = \frac{ik}{2} (A_t A_c^* - A_t^* A_c), \qquad (4.6a)$$

while from (4.4) the time average of this flux is related to the time average of P,

$$\mu \overline{P} = \overline{ik(A_t A_c^* - A_t^* A_c)}, \qquad (4.7)$$

where an overbar represents a time average. With the mean shear different from zero a direction in y is chosen, breaking the mirror symmetry between plus and minus y, so it is not too surprising that a rectified thickness flux in one or the other direction becomes possible.

Figure 5a shows $P(t)$ in the equilibrated finite-amplitude oscillation. Its mean value is clearly different from zero. In Fig. 5a, the oscillation frequency of the shear is chosen to match 2σ, which now depends on G,

$$\sigma = \frac{k\beta F}{K^2(K^2 + 2F)} \left[1 - G^2 \frac{K^4(4F^2 - K^4)}{4F^4} \right]^{1/2}. \qquad (4.8)$$

Note that, as long as $G < 1$, σ remains real. Carrying out such calculations over the range of G between 0 and 0.95 yields the mean value of the thickness flux or the time mean of P as a function of G and is shown in Fig. 5b. The mean value is zero for $G = 0$, as in the small H
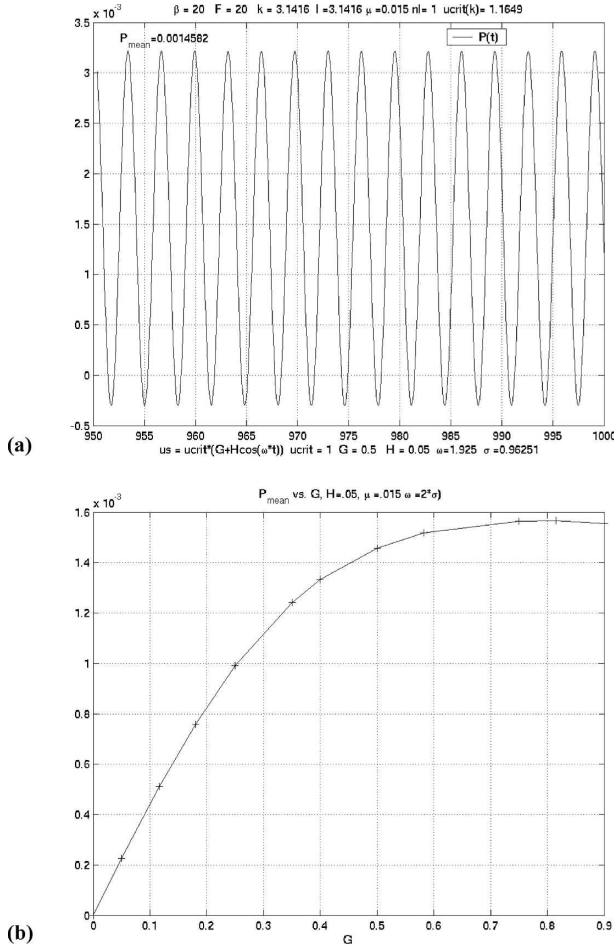
(a)

(b)

FIG. 5. (a) The finite-amplitude oscillation as predicted by the single-mode truncation for $\mu = 0.015$, $F = \beta = 20$, $H = 0.05$ with $\omega = 1.925$ (2σ) for $G = 0.5$. The mean value of P over the oscillation is 1.4582×10^{-3}. (b) The mean of P vs G.

theory, and grows as G increases. Note that over the range of G considered the basic shear is always less than the critical value for all time. Nevertheless, the presence of the oscillating shear, although possessing no mean value, is able to generate a mean thickness flux if there is even a small steady component to the shear. This implies that shears whose mean values are subcritical and whose instantaneous values are also subcritical can nonetheless produce mean thickness (heat) fluxes and produce changes to the time-mean zonal flow.

5. Symmetry breaking and the double-mode solution

The basic flow that we are considering is independent of y and the parameters have been chosen so that only the lowest cross-stream mode, $\sin\pi y$, is unstable. This leads to a finite-amplitude solution that remains symmetric about the midpoint of the channel and possesses the same symmetry as the basic flow. We became aware, by considering the fully nonlinear quasigeostrophic system discussed in section 6, that this symmetry can be broken by the apparently spontaneous emergence of an antisymmetric cross-stream mode with a $\sin2\pi y$ structure. It is important to note that this structure is itself stable on the basic shear flow.

To consider this in the simplest context we construct a simple truncation that permits a double-mode structure. We thus attempt a wave and mean flow correction representation as follows:

$$\phi_c = A_{c1}e^{ikx}\sin ly + A_{c2}e^{ikx}\sin2ly + * + U_{c1}\cos ly/l$$
$$+ U_{c2}\cos2ly/2l \quad \text{and} \tag{5.1a}$$

$$\phi_t = A_{t1}e^{ikx}\sin ly + A_{t2}e^{ikx}\sin2ly + * + U_{t2}\cos2ly/2. \tag{5.1b}$$

Note that the mean flow correction for the barotropic flow, completely absent for the single-mode truncation, though now present, lacks the term in $\cos ly$. This, if present, would provide a correction to the total momentum in the x direction when integrated over the cross-sectional areas of the flow, and, in the absence of an external applied force, that is an impossibility. Also, because of the greater complexity of the two-mode expansion we have approximated the mean flow corrections as just sine functions for the zonal velocity, which, although satisfying the correct boundary condition, is less accurate than the representation of (4.3). However, checking the results against the single-mode calculation when only a single mode is present yields very similar results to the previous representation. Inserting (5.1a, b) into (2.6) and retaining terms of the form of (5.1a, b) yield evolution equations for the wave amplitudes A_{c1}, A_{c2}, A_{t1}, and A_{t2} as well as the amplitudes of the mean flow corrections: U_{t1}, U_{t2}, U_{b2}. These equations are found in appendix B.

$\rightarrow$

FIG. 6. (a) The evolution of the total enstrophy (solid line) and the enstrophy of the second cross-stream mode (dashed line) using the double-mode expansion. For $\mu = 0.015$, $F = \beta = 20$, $H = 0.08$, and $k = l = \pi$. (b) The second-mode amplitudes (absolute values): (upper) the barotropic mode and (lower) baroclinic. (c) As in (b) but for the first mode. (d) The evolution of the amplitudes of the mean flow corrections. The solid line is for the baroclinic correction with the $\sin\pi y$ structure for the velocity, the dashed line is for the baroclinic structure proportional to $\sin2\pi y$, and the dense solid line is the barotropic correction to the zonal flow with structure $\sin2\pi y$.
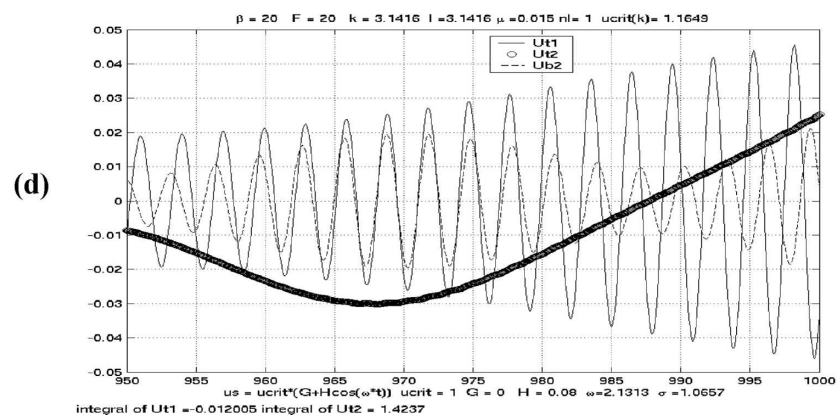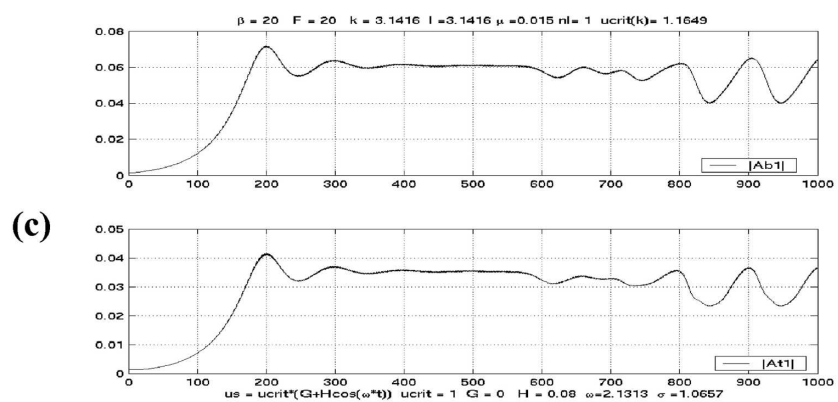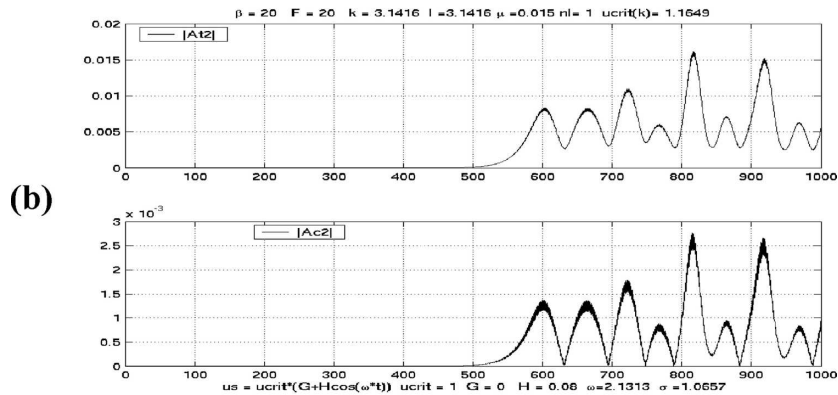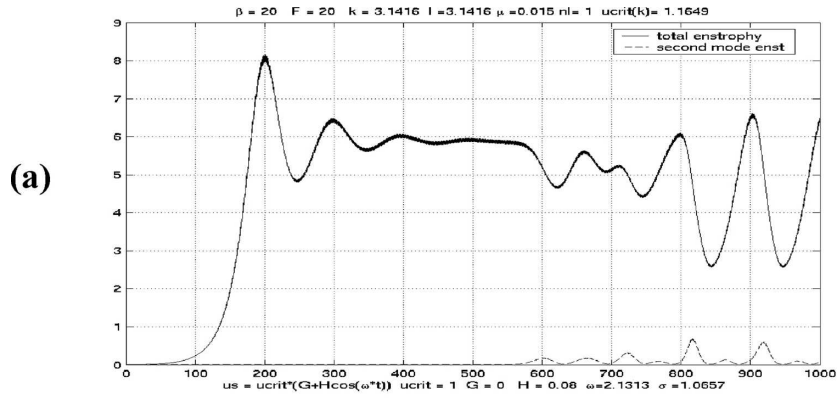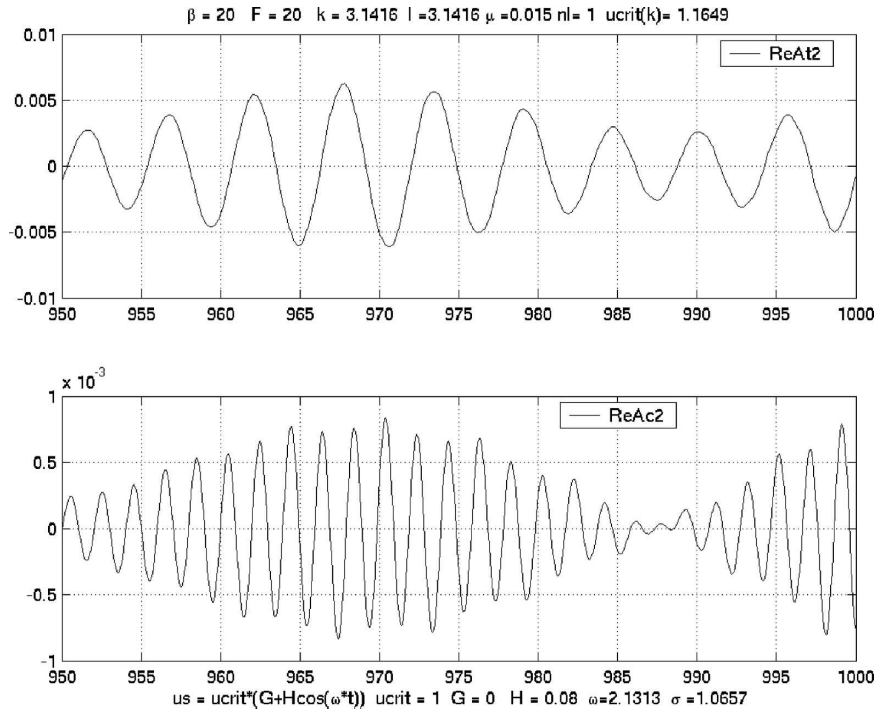
FIG. 7. The oscillation of the second-mode amplitudes in the equilibrated state: (top) The real part of the barotropic mode and (bottom) the baroclinic mode.

We integrate these equations forward with initial conditions for the primary wave as before (values of 0.001 for the real part of the barotropic and baroclinic amplitudes) and now add a very small (10^{-8}) perturbation in the barotropic component of the second mode. Figure 6a shows the evolution of the enstrophy for $G = 0$, $H = 0.08$. The solid line is the total enstrophy and should be compared with Fig. 1a. For short times the evolution is qualitatively similar to the single-mode dynamics. At time $O(600)$ the emergence of the second mode is apparent as the dashed curve and the total enstrophy begins to undergo strong oscillations. Figure 6b shows the emergence of the barotropic and baroclinic components of the second cross-stream mode (the absolute values of the amplitudes are shown) while Fig. 6c shows the evolution of amplitudes for the first cross-stream mode. Accompanying the emergence of the second cross-stream wave structure is the correction to the mean zonal velocity. Figure 6d shows the amplitude evolution of the baroclinic and barotropic corrections to the mean flow, and, now that there are two modes involved, there is a barotropic contribution to the zonal flow. Note that this barotropic flow has a zero average value when integrated across the channel.

The emergence of the second mode appears to be due to an instability of the primary wave of the type discussed by (Kim 1978). Detailed examination of the frequency with which each of the modes oscillates shows that the primary mode has frequencies corresponding to the baroclinic and barotropic Rossby waves expected for small H at the given wavenumbers. On the other hand, the second mode oscillates with frequencies (see Fig. 7) that are not free Rossby wave frequencies but are consistent with an interaction between the first and second modes and the mean flow corrections as described by the equations in appendix B and hence an instability of the first mode to the second mode. The presence of the oscillating subcritical shear introduces a nascent spectral spread in the resulting spectrum waves originating in the parametric instability and a qualitatively significant alteration in the structure of the mean flow.

For smaller values of H the second mode does not appear and the initial condition of the second mode decays. The critical value of H using the model outlined in appendix B is approximately $H = 0.075$ although this value is somewhat sensitive to the model used for the calculation.

6. Fully nonlinear experiments

With the insights gained from the weakly nonlinear and the truncated model, let us now examine results from fully nonlinear numerical runs. These are not sub-
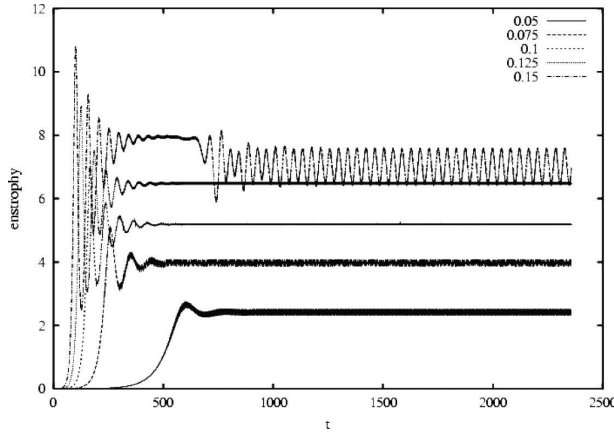
FIG. 8. Eddy enstrophies from the full model for $H = 0.05$, 0.075, 0.1, 0.125, and 0.15 showing the equilibration at larger values as H increases and, for $H = 0.15$, the oscillations associated with the instability to the second zonal mode.
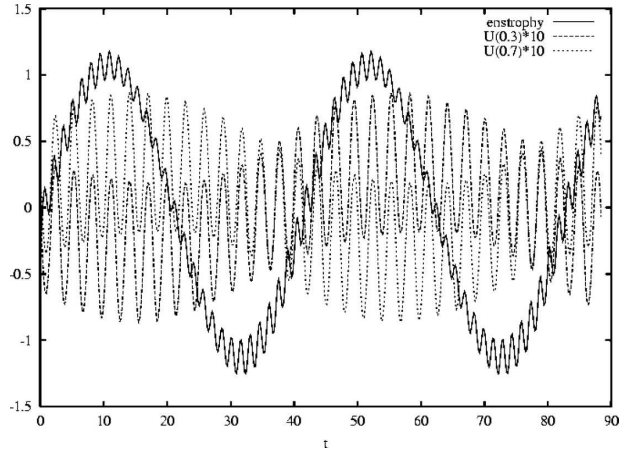

FIG. 9. The time history at $H = 0.15$ of the enstrophy (solid line, mean subtracted), the baroclinic zonal velocity correction at $y = 0.3$ (dashed line) and at $y = 0.7$ (dotted line) illustrating the symmetry breaking of the mean flow and the north–south migration of flow axis.

ject to the assumptions and limitations of the previous sections so that we can determine the degree to which the simpler models apply and when they begin to fail. As we shall see, even at small forcing amplitudes, the changes in mean flows quickly develop a more complex meridional structure as well as barotropic components. Shortly after the symmetry breaking point, the flows become irregular with fluctuation energy spreading into more and more scales, and turbulence can result. We begin with a series of experiments forced at the critical frequency

$$\omega = \frac{\beta k}{K^2} - \frac{\beta k}{K^2 + 2F} \qquad (6.1)$$

(period $T_f = 2\pi/\omega$) and gradually increasing amplitudes. The parameters are $\beta = F = 20$ and $k = l = \pi$. The critical forcing amplitude from (3.11) is $H = 0.033$, and numerical experiments for $H = 0.025$, 0.03, and 0.035 are consistent with this value. For small but supercritical values of $H \leq 0.125$, the eddy enstrophies stabilize with an oscillation at 2 times the frequency ω of the forcing (Fig. 8). At $H = 0.15$, the symmetry-breaking instability has developed, and the enstrophy develops an oscillation with a period of about 14 times the forcing period in addition to the faster, smaller-amplitude variations at 2ω.

In the zonal means, we also see a transition from symmetric states with the period of the basic forcing to nonsymmetric flows. Figure 9 illustrates the cycle of eddy enstrophy and the zonal flow corrections at $y = 0.3$ and $y = 0.7$; both the cycling at ω and the long-term oscillation with the mean flow shifting regularly north and south are evident. To see the changes more clearly,

we construct series of $U(y, n \times T_f)$. The sequence of these snapshots taken when the forcing is maximum demonstrates the change in character between $H = 0.125$ and $H = 0.15$ (Fig. 10). In addition, we see two complications not arising in the truncated model: first, the shear correction becomes less peaked and then develops a double structure at $H = 0.125$, and, second, significant barotropic zonal flow corrections are also generated. These changes may account for the delayed onset of the symmetry breaking instability compared with the truncated model (H between 0.125 and 0.15 rather than near 0.075); however, the fact that it appears in the simpler model would argue that the basic mechanism is still an instability of the waves. Even at small values of H, contours of ψ do show the phase tilts with y necessary to produce barotropic flows.

For larger values of H, 0.175 and 0.2, the changes from period to period become chaotic (Fig. 11). Likewise, the spectrum of the eddies shows significant energy in modes other than $k = \pi$; to illustrate this, we have computed the spectrum (periodogram) of q'_1 along the centerline of the channel and have taken the ratio of enstrophy in modes at wavenumbers greater than the primary $k > \pi$ to the total (Fig. 12). The energy in higher harmonics jumps slightly as we reach these more chaotic states; in addition, the y structures become much more irregular. The $H = 0.2$ run eventually (after about $1600T_f$) settles into a state like that described next for large H and remains in that state thereafter. The $H = 0.175$ experiment has been extended to $3200T_f$ and remains in the regime with the asymmetric mean flow, sometimes strong in the north and sometimes in
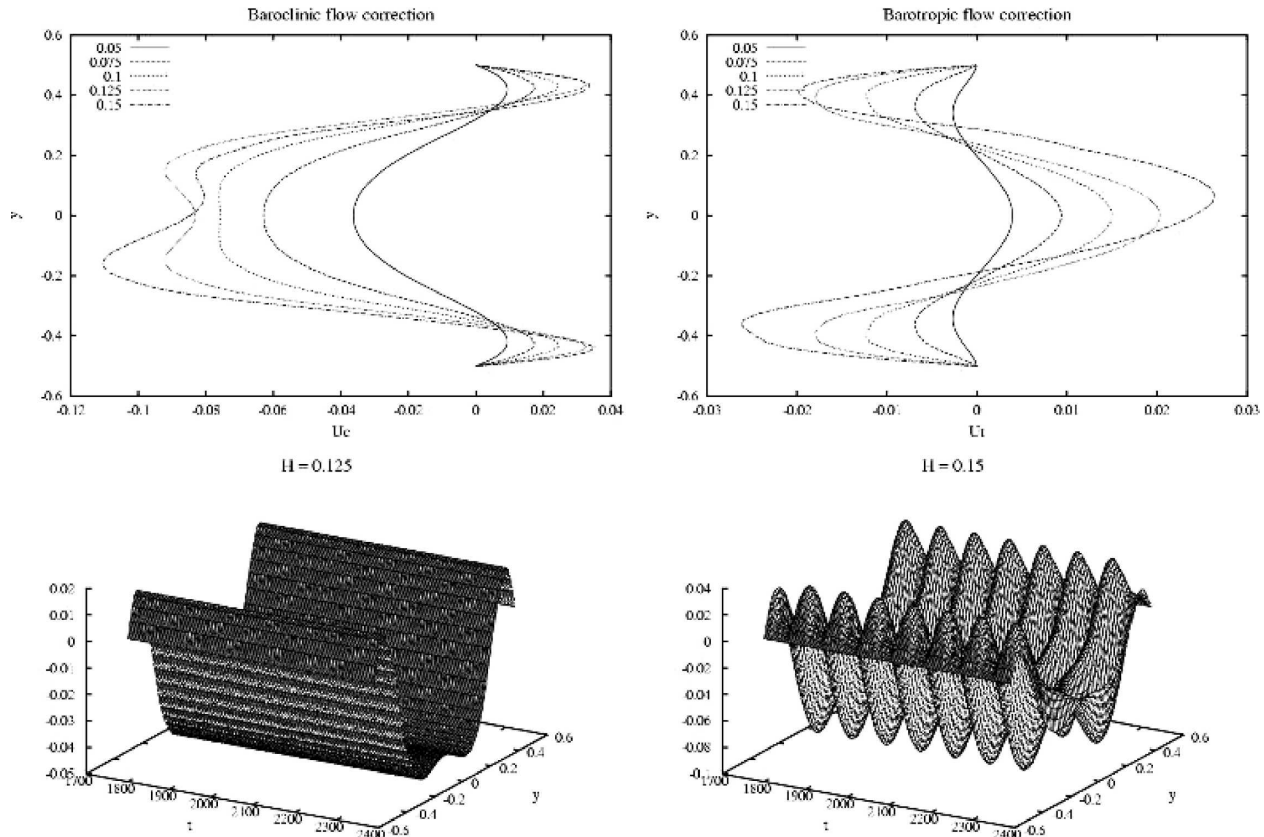
FIG. 10. Meridional structure of the zonal flow corrections at the time of maximum forcing for $H = 0.05$, 0.075, 0.1, 0.125, and 0.15. The last two cases are plotted as functions of time as well, with snapshots taken at $t = nT_f$. The negative values for $H = 0.125$ indicate that the eddies decrease the shear, stabilizing the flow. The structure oscillates with the period of the forcing (exactly in the small-H case).

the south. The flow can remain in one regime for several hundred forcing periods, implying significant periods of northward or southward eddy heat fluxes. (For reference, the damping time, μ^{-1} is only 23 forcing periods.)

As the forcing amplitude is increased further ($H = 0.225$, 0.25), another transition occurs and the eddy enstrophy becomes very large (Fig. 13), but the zonal flow corrections become more stable with most of the shear occurring in thin regions near the walls (Fig. 14). The enstrophy spectra are now much flatter, indicating that the flow has indeed become turbulent. The potential vorticity (Fig. 15) has multiple filaments of high and low PV drawn away from the walls by the large eddies. Movies from these experiments (available at http://lake.mit.edu/~glenn/joe/movies.html) show that the eddies strengthen and weaken irregularly.

In the previous experiments, the unstable mode had a wavenumber of π corresponding to the longest wave in the numerical channel (which has $L_x = 2$, $L_y = 1$). Figure 16 shows the growth rates for different down-stream modes for a higher value of $F = 50$. By choosing the frequency of the forcing, we can excite a higher mode, leaving the possibility of an upscale cascade of energy as the wave reaches finite amplitude. We have taken two cases with $\omega = 2.403$ and $H = 0.1$ or 0.15. The eddy enstrophies are shown in Fig. 17. In the lower-amplitude case, the wave grows and then breaks, developing smaller-amplitude, irregular, larger-scale waves. The waves equilibrate, presumably balancing weak energy input in mode three with upscale cascade and dissipation.

For the larger-amplitude forcing (still very far below the range where modes 1 and 2 could grow by themselves), the final state is much more turbulent, as shown in the potential vorticity snapshots (Fig. 18). The β term still dominates the mean PV gradients, but the zonal flows show substantial higher mode variability (Fig. 19). Once again, we see turbulent eddies maintained even when the forcing is less than 20% of the amplitude required to reverse the PV gradient in one of the layers.
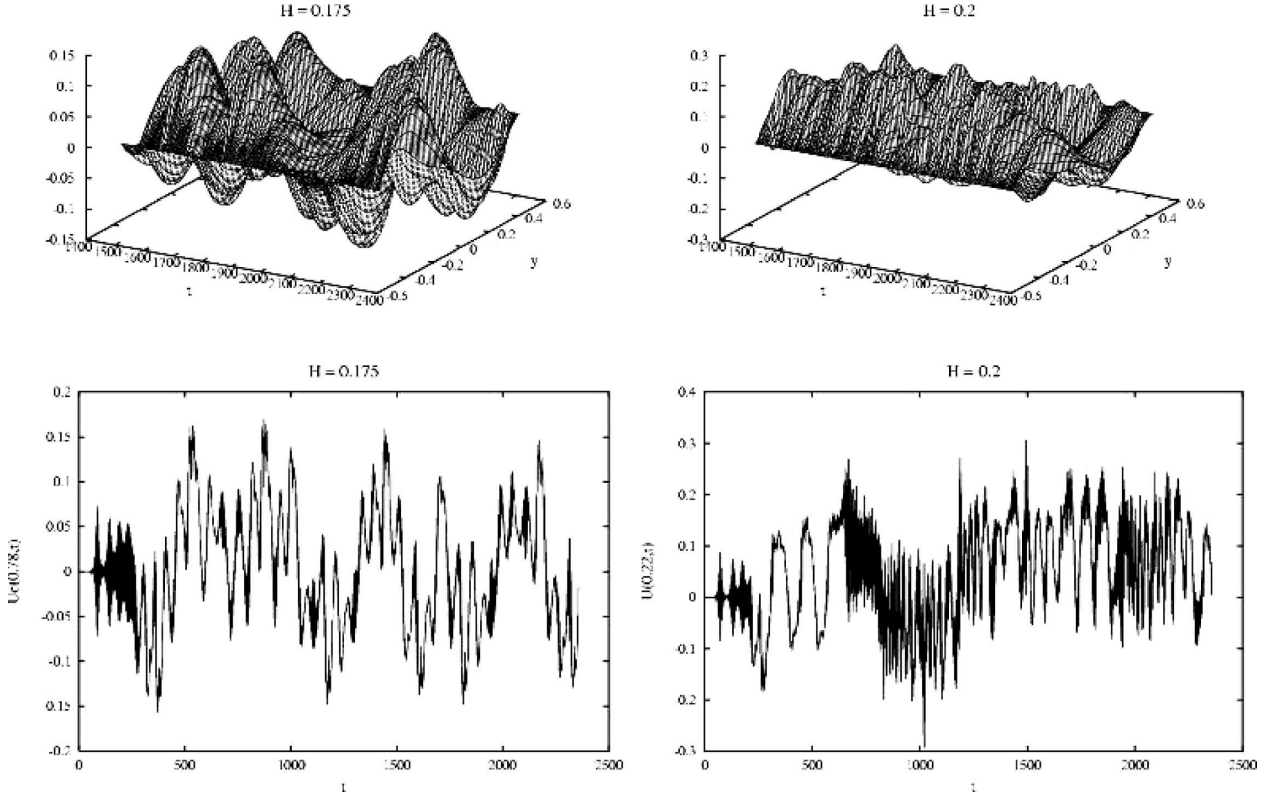
FIG. 11. (top) Mean baroclinic flow corrections for $H = 0.175$ and 0.2 at times nT_f. (bottom) Time series at particular y values; the early stages represent the growth of the instability and the transitions to asymmetric zonal flows.

7. $\beta = 0$: Nonlinear instability

We have so far considered oscillating flows that are deeply subcritical to the classical, steady flow, linear instability criterion because of the presence of the β effect. We now consider the opposite situation to demonstrate the role of nonlinearity in enabling the waves to develop: just as in the case when the forcing frequency is above the cutoff value, finite-amplitude effects can be crucial. If $\beta = 0$ no shear threshold exists but it is easy to show that the purely oscillating shear ($G = 0$) is formally linearly stable. Consider the linear version of (2.6) with $\beta = 0$,

$$\left(\frac{\partial}{\partial t} + \mu\right)(\nabla^2 \phi_c - 2F\phi_c) + \frac{U_s}{2}\frac{\partial}{\partial x}(\nabla^2 \phi_t + 2F\phi_t) = 0,$$

(7.1a)

$$\left(\frac{\partial}{\partial t} + \mu\right)\nabla^2 \phi_t + \frac{U_s}{2}\frac{\partial}{\partial x}\nabla^2 \phi_c = 0, \quad \text{and} \quad (7.1b)$$

$$U_s = U_o \cos\omega t. \quad (7.1c)$$

The dissipation can be removed from the problem by the transformation,

$$\begin{pmatrix} \phi_t \\ \phi_c \end{pmatrix} = e^{-\mu t}\begin{pmatrix} \varphi_t \\ \varphi_c \end{pmatrix}. \quad (7.2)$$

If the basic shear again has the form, $U_s = U_o \cos\omega t$, the problem can further be reduced to the steady version by the transformation of the time variable as

$$\tau = \frac{\sin\omega t}{\omega}, \quad (7.3)$$

a special case of the transformation $d\tau/dt = \text{const } U_s(t)$. The linear problem for φ_c, φ_t becomes

$$\left(\frac{\partial}{\partial \tau}\right)(\nabla^2 \varphi_c - 2F\varphi_t) + \frac{U_o}{2}\frac{\partial}{\partial x}(\nabla^2 \varphi_t + 2F\varphi_t) = 0 \quad \text{and}$$

$$\left(\frac{\partial}{\partial \tau}\right)\nabla^2 \varphi_t + \frac{U_o}{2}\frac{\partial}{\partial x}\nabla^2 \varphi_c = 0, \quad (7.4)$$

which is precisely the same as the linear, inviscid problem for the constant shear U_o. This reduction of the linear problem to the steady case has been discussed by Hart (1971). The solution to that classical problem (Pedlosky 1987) has a perturbation growth rate

$$\sigma_g = \pm \frac{kU_o}{2}\left(\frac{2F - K^2}{2F + K^2}\right)^{1/2}. \quad (7.5)$$
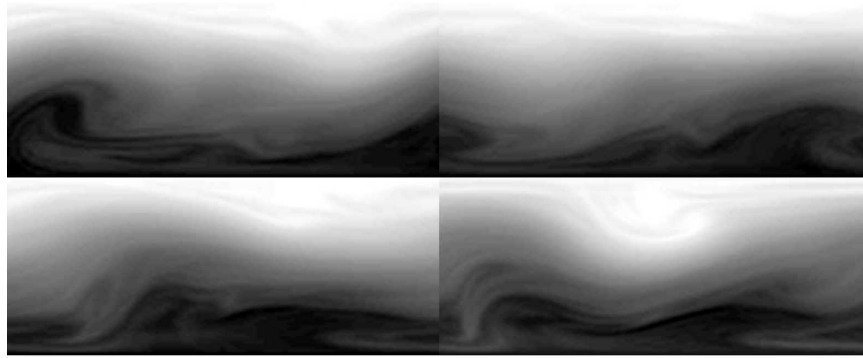
(a)
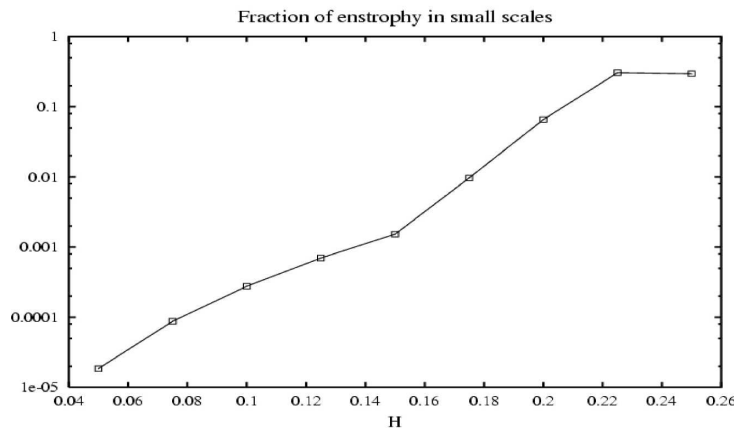
(b)

FIG. 12. (a) Images showing the potential vorticity in the upper layer for $H = 0.2$ over one forcing period (from left to right, top to bottom). (b) Fraction of enstrophy in the higher harmonics $k = n\pi$ with $n \geq 2$ as a function of forcing amplitude H.

This yields an exponential growth (or decay) in the variable τ. However, in the original variable, t, the evolution with time will be

$$\begin{pmatrix} \phi_t \\ \phi_c \end{pmatrix} = e^{-\mu t} \left[e^{\sigma_g \sin\omega t/\omega} \begin{pmatrix} A_{t+} \\ A_{c+} \end{pmatrix} \right.$$
$$\left. + e^{-\sigma_g \sin\omega t/\omega} \begin{pmatrix} A_{t-} \\ A_{c-} \end{pmatrix} \right] e^{ikx} \sin ly. \qquad (7.6)$$

Since the factor $\sin\omega t/\omega$ is periodic in time, the exponential terms in (7.6) proportional to σ_g will only temporarily each grow or decay but there will be no long-term change over a period of the oscillating shear. Indeed, in the presence of dissipation the linear disturbance is destined to always eventually decay and this will be true regardless of the size of U_o. Note, though, that, if U_s had a mean value with a nonzero time average, this term could give exponential growth that could balance the dissipation.

Figure 20a shows the enstrophy evolution, using the single-mode truncation, for $\beta = 0$, $\mu = 0.015$ $F = 20$, $H = 0.4$, and $k = l = \pi$ and $\omega = 0.1$ for the linear

problem with the shear (7.1c). As anticipated, although σ_g is positive, (0.4486) and exceeds μ, the solution decays with time. Had μ been zero, the solution would be perfectly periodic. Nevertheless, there is an initial period of growth when the positive root for σ_g yields ephemeral exponential growth and the amplitude can
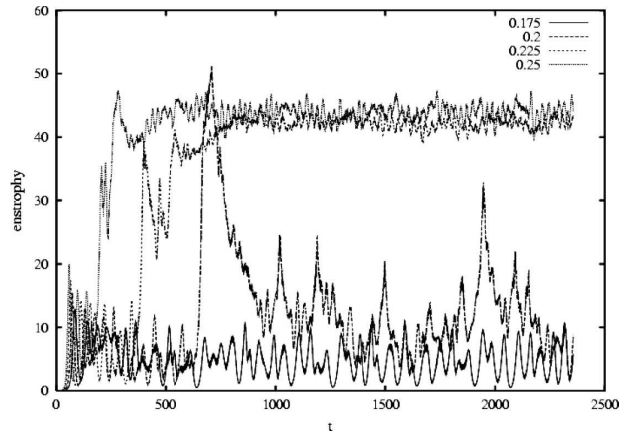

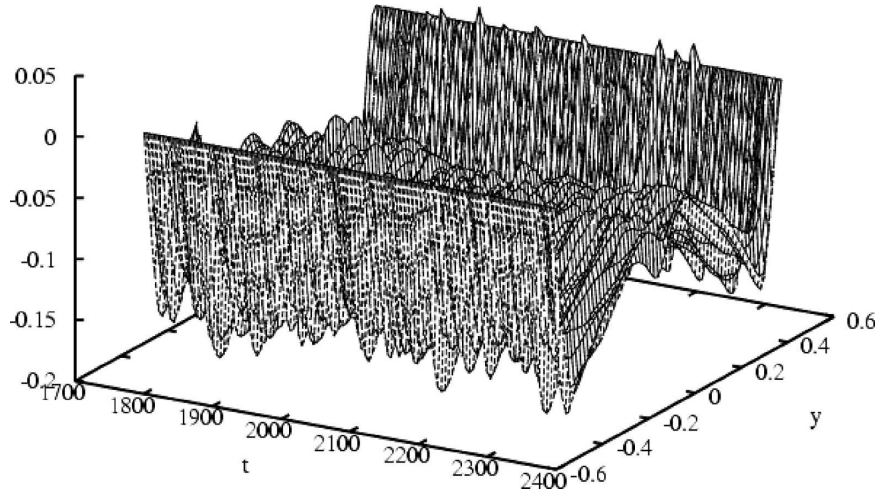FIG. 13. Eddy enstrophies for $H = 0.175$, 0.2, 0.225, and 0.25.

FIG. 14. Zonal mean correction time series for $H = 0.25$ at times nT_f. Again, these oscillate between negative (shown) and positive values during each forcing period, T_f.

become temporarily quite large. In doing so, the mean flow correction to the linear problem no longer becomes negligible. Two factors can then enter to alter the evolution. If the mean flow correction has a mean value, one might expect the possibility of instability simply due to the presence of a constant term in the transformation, $d\tau/dt = \text{const} \times U_s(t)$, presuming the mean flow correction can heuristically be considered as a simple alteration of the basic flow. Similarly, if the phasing of the mean flow correction mixes the two modes with $\pm\sigma_g$, the initially growing mode corresponding to $+\sigma$ can be transferred to the mode of the opposite sign, $-\sigma_g$, a half period later and so continue to grow. Figure 20b shows the function $P(t)$ [see (4.3)] over two periods of the basic oscillation calculated using the linear solution in the inviscid limit. Note that the mean value is not zero, and it is therefore of interest to see whether the nonlinear solution including this effect will remain stable and decay due to dissipation. Figure 20c shows the enstrophy in the full nonlinear solution in which the mean flow correction is allowed to react back

on the developing perturbation. A comparison with Fig. 20a shows the destabilization of the linear solution by the nonlinear wave–mean flow interaction. The enstrophy after a period of exponential growth now maintains itself against dissipation. Thus, even in the case where the linear problem is stable, the nonlinear dynamics of the purely oscillating shear flow is unstable, leading to persistent finite-amplitude perturbations even in the presence of dissipation. The result is, clearly, a function of the initial conditions for the perturbations. If the initial conditions are too small, the perturbation will never grow to a large enough amplitude for the nonlinear effects to be destabilizing before the dissipation damps the solution to zero. Figure 20d shows the function $P(t)$ for the fully nonlinear solution along with the
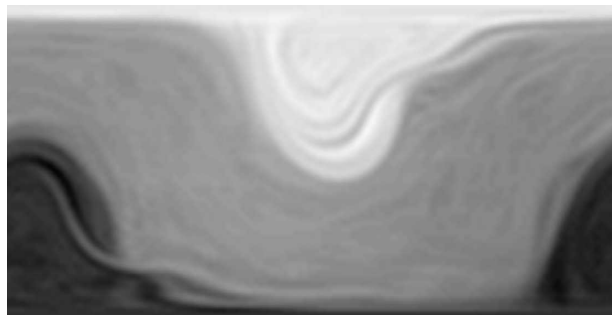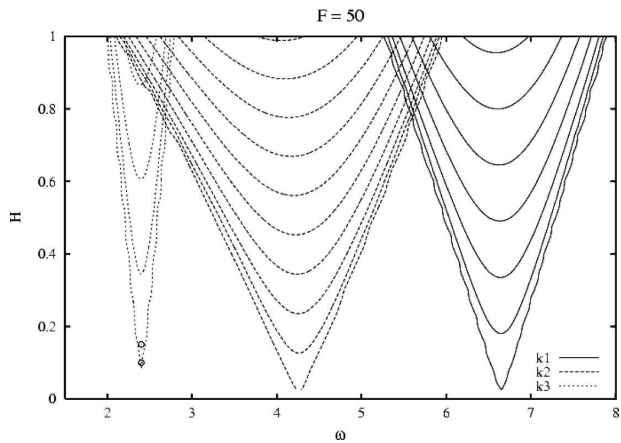

FIG. 16. Linear growth rates as a function of ω and H for modes $k = \pi, 2\pi,$ and 3π. Contour intervals are 0.05, 0.1, and 0.1, respectively, for the modes $k = \pi, 2\pi,$ and 3π. The dots in the figure show locations for calculations mentioned in the text.

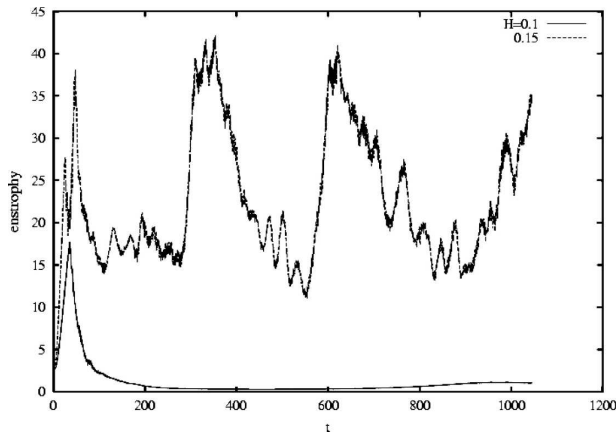FIG. 15. Snapshot of the total q_1 field.

FIG. 17. Enstrophies for low-frequency forcing that excites mode $k = 3\pi$. The forcing amplitudes are small: $H = 0.1$ and 0.15.

shear flow shown in the dashed line. As before, when P is positive the correction to the shear in the center of the channel where the perturbation is greatest is opposite in sign to the basic shear, and this is clearly a stabilizing effect. We note that over most of the cycle of the nonlinear solution that this is precisely what happens. However, there are brief periods at the start of each cycle where the shear correction reinforces the basic shear and it is at this interval, we believe, that the two linear modes become mixed, allowing continued energy extraction against dissipation.

8. Conclusions and discussion

Zonal flows that are deeply subcritical with respect to the classical threshold for baroclinic instability (Pedlosky 1987) in the two-layer model are destabilized

when the flow is time dependent. The fundamental mechanism is a parametric instability and this, in turn, is closely related to the release of energy in growing nonnormal modes of instability (Farrell and Ioannou 1999). We have concentrated on the resulting nonlinear dynamics in finite amplitude and have found a wide range of behavior. Earlier work by Pedlosky and Thomson (2003) focused on the weakly nonlinear behavior near the conventional marginal curve for instability and much of the chaotic behavior of the dynamics resulted from episodic crossings into the supercritical regime of the conventional problem. We emphasize that in this study the shears are far weaker than in the Pedlosky and Thomson paper and the basic shear is deeply subcritical according to the conventional criterion. The potential vorticity gradients in both layers remain positive and $O(1)$.

For very weak shear, analytic, asymptotic solutions show that the growing instability equilibrates to barotropic and baroclinic waves with amplitudes proportional to $H^{1/2}$ and a frequency shift proportional to H. The two waves produce oscillating heat fluxes and mean shear changes on the order H: these reduce the effective parametric instability and yield an equilibrated state in which the energy released by the instability is balanced by dissipation. The finite-amplitude response is also obtained for parameter values for which parametric instability is absent in linear theory so that the effect of nonlinearity is to extend the frequency range of the finite-amplitude instabilities.

A truncated wave model is used to extend these results to consider alterations in the dynamics when the mean shear has a steady component and demonstrates that, in the presence of a time mean shear, the insta-
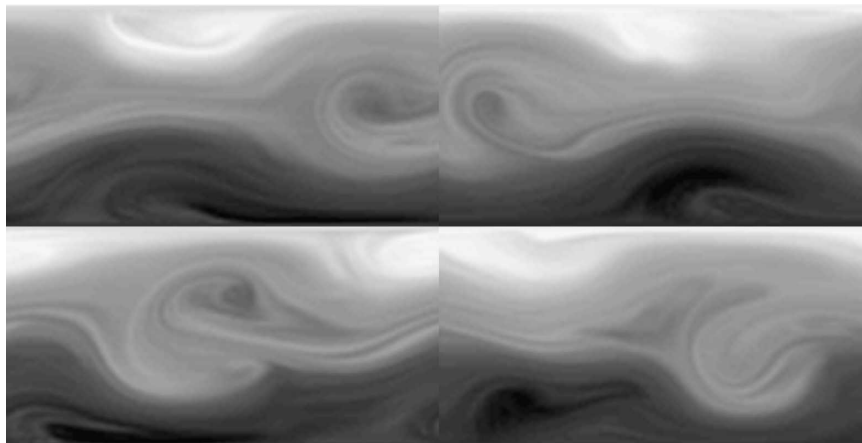

FIG. 18. Snapshots of the potential vorticity from the $H = 0.15$ numerical experiment. Each panel is separated by $T_f/2$. The two left panels in a vertical plane are one period apart and clearly show significant variations.
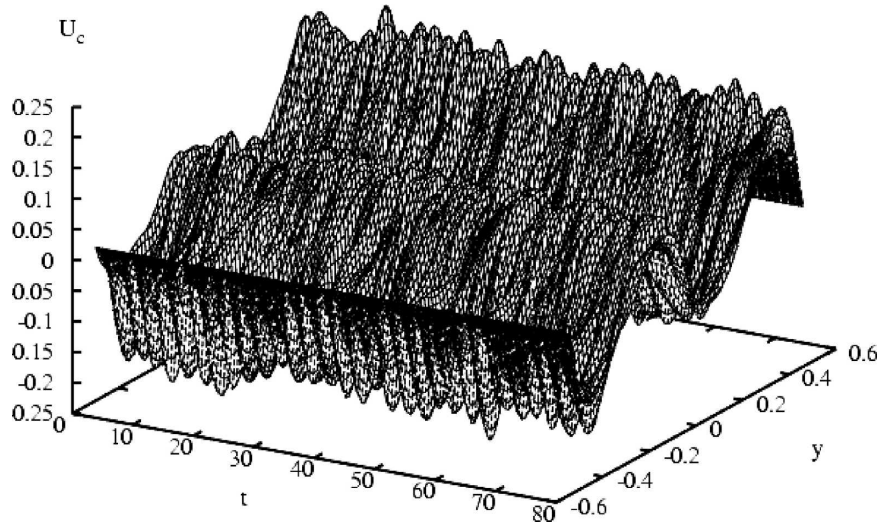
FIG. 19. Zonal flow profiles for $H = 0.15$. The plot shows 30 forcing periods with 16 samples per period (unlike Figs. 10, 11, and 14).
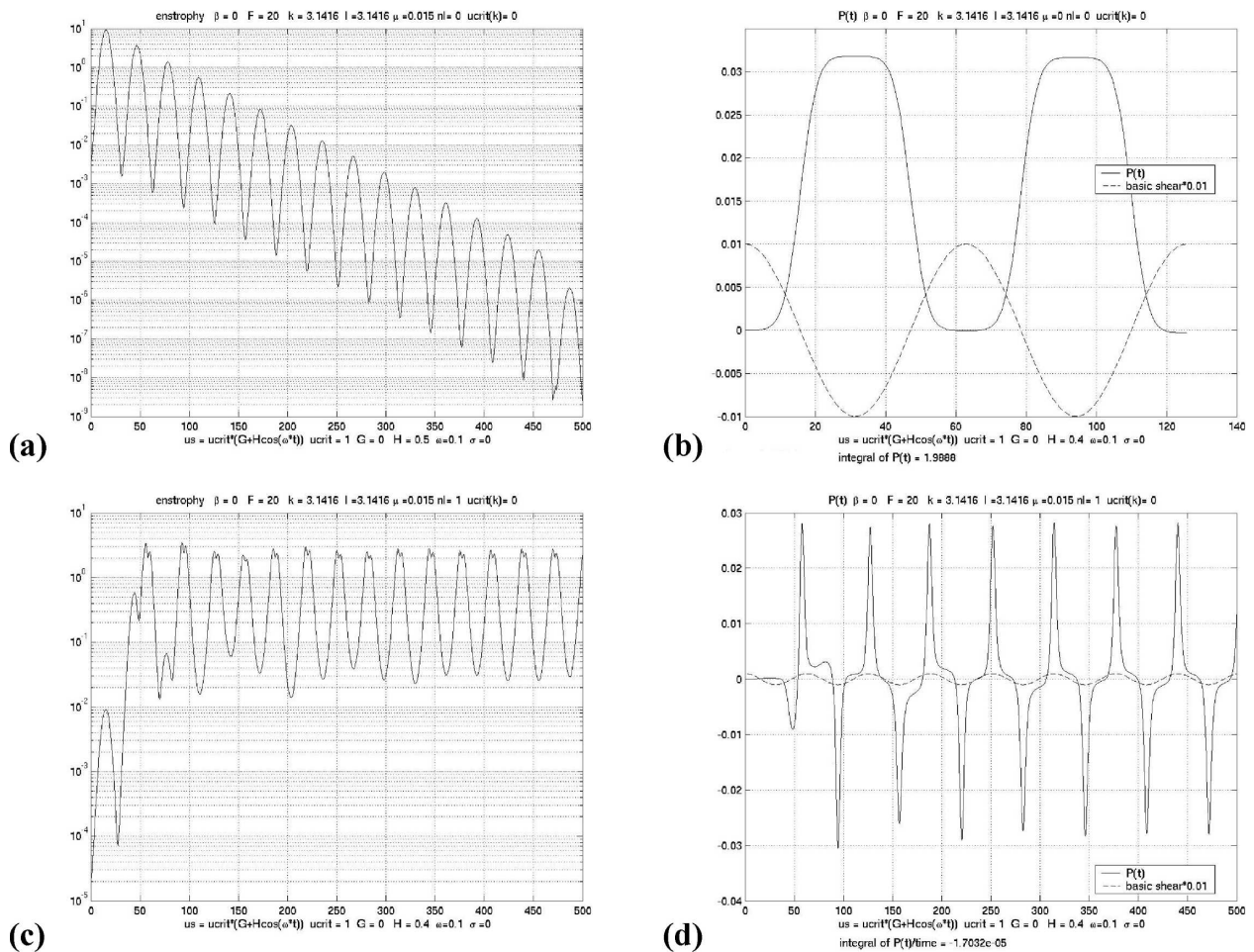

FIG. 20. Evolution of the enstrophy for (a) the linear and (c) the nonlinear problem when $\beta = 0$, $\mu = 0.015$, $F = 20$, $H = 0.4$, and $k = l = \pi$ and $\omega = 0.1$. The function $P(t)$ calculated with (b) the linear inviscid and (d) the nonlinear solution.

bility produces a time-mean eddy heat flux and heat flux convergence, even though the shear at each instant is (classically) stable. The truncated model also demonstrates an interesting symmetry breaking in which the mean flow, originally symmetric about its center line, develops an asymmetric component representing a meandering of the jet axis of the flow from high to low latitudes.

These analytical and quasi-analytical results are extended to higher-amplitude motions with a fully nonlinear quasigeostrophic model. When the shear is, at each instant, very small, the nonlinear model yields results in qualitative agreement with the analytical models. However, at larger values of the shear, but still classically subcritical, the full model reveals a rich finite-amplitude behavior in which the symmetry breaking, although delayed with respect to the analytical models, enters at the same time with a strong barotropic component to the mean field correction. This production of barotropic mean flow is a higher-order effect in the asymptotic theories and is a fully nonlinear result.

At moderately high values of the instantaneous shear, about one-quarter of the classical critical value, the flow is already strongly turbulent. Other zonal scales of motion, which are stable on the zonal flow, appear. The wavenumber spectrum becomes relatively flat and the field of flow shows strong filaments of high and low potential vorticity. This is manifested clearly in the sudden increase in the overall level of the enstrophy in the solutions. When the unstable mode is not the longest in the system, the nonlinear dynamics produces an upscale cascade of energy with a strongly turbulent flow field. For these turbulent solutions the potential vorticity fluxes drive changes to the mean flow that have time scales very much longer than the oscillation of the basic shear and can be considered to have become rectified in time.

Consequently, we suggest that classically stable flows, in the sense that at each instant the shear lies well below the conventional stability threshold, can in fact become strongly unstable. Highly energetic instability waves and eddies result that strongly alter the mean flow. It follows that the parameter range for which potential energy can be released by baroclinic instability can be substantially broadened by time dependence of the basic state with obvious consequences for the problem of parameterizing the effect of eddies in oceanic and atmospheric flow models.

APPENDIX A

The Coefficients N_1 and N_2

The coefficients N_1 and N_2 in (3.9a, b) are obtained by projecting the nonlinear interaction of the lowest-order wave with correction to the basic flow onto the form of the basic eigenfunctions. A considerable amount of algebra then leads to

$$N_1 = \frac{4l^2 kF}{K^2(4l^2 + 2F)}\left[2l^2 - \frac{K^2}{2} - \frac{8l^2(K^2 + 2F)}{4l^2 + 2F}\frac{\tanh(F/2)^{1/2}}{(F/2)^{1/2}}\right] \quad \text{and} \tag{A.1a}$$

$$N_2 = \frac{4l^2 kF}{(K^2 + 2F)(4l^2 + 2F)}\left[\frac{K^2}{2} - 2l^2 - F + \frac{8l^2(K^2 + 2F)}{4l^2 + 2F}\frac{\tanh(F/2)^{1/2}}{(F/2)^{1/2}}\right]. \tag{A.1b}$$

APPENDIX B

The Evolution Equations for the Two-Mode Expansion

Defining

$$K_1^2 = k^2 + l^2 \quad \text{and} \quad K_2^2 = k^2 + 4l^2, \tag{B.1a, b}$$

the evolution equations for the two-mode expansion amplitudes are, for the waves:

$$\left(\frac{\partial}{\partial t} + \mu\right)A_{t1} = \frac{-ikU_s}{2}A_{c1} + i\frac{k\beta}{K_1^2}A_{t1} + ik\frac{(4l^2 - K_2^2)}{K_1^2 l}\frac{32}{15}A_{t2}U_{t2} + ik\frac{(l^2 - K_1^2)}{K_1^2 l}\frac{8}{3}A_{c1}U_{c2} + ik\frac{(4l^2 - K_2^2)}{K_1^2 l}\frac{32}{15}A_{c2}U_{c2},$$

$$(B.2a)$$

$$\left(\frac{\partial}{\partial t} + \mu\right)A_{t2} = \frac{-ikU_s}{2}A_{c2} + i\frac{k\beta}{K_2^2}A_{t2} + ik\frac{(4l^2 - K_1^2)}{K_2^2 l}\frac{32}{15}A_{t1}U_{t2} + ik\frac{(l^2 - K_2^2)}{K_2^2 l}\frac{32}{15}A_{c2}U_{c1}$$

$$+ ik\frac{(4l^2 - K_1^2)}{K_2^2 l}\frac{32}{15}A_{c1}U_{c2}, \tag{B.2b}$$

$$\left(\frac{\partial}{\partial t} + \mu\right)A_{c1} = \frac{ikU_s}{2}\frac{2F - K_1^2}{2F + K_1^2}A_{t1} + i\frac{k\beta}{K_1^2 + 2F}A_{c1} - ik\frac{(K_1^2 - 2F - l^2)}{(K_1^2 + 2F)l}\frac{8}{3}A_{t1}U_{c1} - ik\frac{(K_2^2 - 2F - 4l^2)}{(K_1^2 + 2F)l}\frac{32}{15}A_{t2}U_{c2}$$

$$- ik\frac{(K_2^2 + 2F - 4l^2)}{(K_1^2 + 2F)l}\frac{32}{15}A_{c2}U_{t2}, \quad \text{and} \tag{B.2c}$$

$$\left(\frac{\partial}{\partial t} + \mu\right)A_{c2} = \frac{ikU_s}{2}\frac{2F - K_2^2}{2F + K_2^2}A_{t2} + i\frac{k\beta}{K_2^2 + 2F}A_{c2} - ik\frac{(K_1^2 - 2F - 4l^2)}{(K_2^2 + 2F)l}\frac{32}{15}A_{t1}U_{c2} - ik\frac{(K_2^2 - 2F - l^2)}{(K_2^2 + 2F)l}\frac{32}{15}A_{t2}U_{c1}$$

$$- ik\frac{(K_1^2 + 2F - 4l^2)}{(K_2^2 + 2F)l}\frac{32}{15}A_{c1}U_{t2}, \tag{B.2d}$$

while for the mean flow corrections:

$$\left(\frac{\partial}{\partial t} + \mu\right)U_{c1} = -\frac{ik2Fl}{(2F + l^2)}\frac{8}{3}(A_{t1}A_{c1}^* - A_{t1}^*A_{c1}) - \frac{ik4Fl}{(2F + l^2)}\frac{16}{15}(A_{t2}A_{c2}^* - A_{t2}^*A_{c2}), \tag{B.3a}$$

$$\left(\frac{\partial}{\partial t} + \mu\right)U_{c2} = -\frac{ikl}{(2F + 4l^2)}\frac{128}{15}(A_{t1}A_{c2}^* - A_{t1}^*A_{c2})(2F + K_2^2 - K_1^2) - \frac{ikl}{(2F + 4l^2)}\frac{128}{15}(A_{t2}A_{c1}^* - A_{t2}^*A_{c1})(2F + K_1^2 - K_2^2), \tag{B.3b}$$

and

$$\left(\frac{\partial}{\partial t} + \mu\right)U_{t2} = \frac{ikl}{4l^2}\frac{128}{15}(K_1^2 - K_2^2)(A_{t1}A_{t2}^* - A_{t1}^*A_{t2}) + \frac{ikl}{4l^2}\frac{128}{15}(K_1^2 - K_2^2)(A_{c1}A_{c2}^* - A_{c1}^*A_{c2}). \tag{B.3c}$$

REFERENCES

Farrell, B. F., and P. J. Ioannou, 1999: Perturbation growth and structure in time-dependent flows. *J. Atmos. Sci.,* **56,** 3622–3639.

Hart, J. E., 1971: A note on the baroclinic instability of general time-dependent basic fields of the Eady type. *J. Atmos. Sci.,* **28,** 808–809.

Kim, K., 1978: Instability of baroclinic Rossby waves: Energetics in a two-layer ocean. *Deep-Sea Res.,* **25,** 795–814.

Pedlosky, J., 1987: *Geophysical Fluid Dynamics.* 2d ed. Springer-Verlag, 710 pp.

——, and J. Thomson, 2003: Baroclinic instability of time-dependent currents. *J. Fluid Mech.,* **490,** 189–215.

Phillips, N. A., 1954: Energy transformations and meridional circulations associated with simple baroclinic waves in a two-level geostrophic model. *Tellus,* **6,** 273–286.

Poulin, F. J., G. R. Flierl, and J. Pedlosky, 2003: Parametric instability in oscillatory shear flow. *J. Fluid Mech.,* **481,** 329–353.

Shepherd, T. G., 1983: Mean motions induced by baroclinic instability in a jet. *Geophys. Astrophys. Fluid Dyn.,* **27,** 35–72.